

Article

Influence of Urban Spatial Structure on the Spatial Distribution of Gaseous Pollutants

Qixin Ren, Baoyan Shan ^{*}, Qiao Zhang and Changkuan Shui

School of Surveying and Geo-Informatics, Shandong Jianzhu University, Jinan 250101, China; 2021165104@stu.sdjzu.edu.cn (Q.R.); 2021165109@stu.sdjzu.edu.cn (Q.Z.); 2022165116@stu.sdjzu.edu.cn (C.S.)
* Correspondence: shan7066@sdjzu.edu.cn

Abstract: The spatial distribution pattern of urban spatial structure affects air flow and local meteorological conditions, which in turn influence the diffusion of air pollutants. This study built the urban spatial structure index system based on DEM, urban road networks, and big data. The ordinary kriging interpolation method was used to analyze the spatial distribution of gaseous pollutant concentrations in Jinan City. Correlation analysis, stepwise regression analysis, and bivariate global spatial autocorrelation analysis were used to study the influence of the urban spatial structure index on the spatial distribution of gaseous pollutant concentration. The main conclusions were as follows: (1) Evident spatial and temporal differences were observed in the concentration distribution of gaseous pollutants in Jinan. The spatial distribution of NO₂ and CO concentrations showed a gradual decrease from north to south. Spatial heterogeneity was observed in the distribution of SO₂ and O₃ concentrations. (2) The urban spatial structure indicators had varying effects on the spatial distribution of different gaseous pollutant concentrations. The important factors that influenced the spatial distribution of urban gaseous pollutant concentrations included terrain elevation, building density, building volume, and floor area ratio. The greater the terrain undulation, the denser the building distribution, the greater the difference in building volume, and the greater the plot ratio, the greater the impact on the diffusion and spatial distribution of urban gaseous pollutants. (3) The spatial distribution of urban gaseous pollutant concentrations was significantly affected by the urban spatial structure indicators in the surrounding areas. Furthermore, the spatial distributions of NO₂, SO₂, CO, and O₃ concentrations had a significant negative spatial correlation with the average DEM and standard deviation of the surrounding adjacent areas and a significant positive spatial correlation with the average and standard deviation of building height, standard deviation of building area, and building density in the surrounding adjacent areas (in June).

Keywords: urban spatial structure; gaseous pollutants; stepwise regression analysis; bivariate global spatial autocorrelation analysis



Citation: Ren, Q.; Shan, B.; Zhang, Q.; Shui, C. Influence of Urban Spatial Structure on the Spatial Distribution of Gaseous Pollutants. *Atmosphere* **2023**, *14*, 1231. <https://doi.org/10.3390/atmos14081231>

Academic Editors: Sumei Liu, Junjie Liu and Wei Liu

Received: 20 June 2023
Revised: 23 July 2023
Accepted: 28 July 2023
Published: 31 July 2023



Copyright: © 2023 by the authors. Licensee MDPI, Basel, Switzerland. This article is an open access article distributed under the terms and conditions of the Creative Commons Attribution (CC BY) license (<https://creativecommons.org/licenses/by/4.0/>).

1. Introduction

With rapid urbanization, urban air pollution has witnessed a steady increase. Long-term exposure to air pollution is known to affect human health and increase the incidence of respiratory ailments [1,2]. Therefore, research on air quality has received extensive attention. NO₂, SO₂, CO, and O₃ are important air pollutants that directly affect human health as well as animal and plant growth [3]. Thus, it is of great practical importance to study the temporal and spatial distribution of these gaseous pollutants as well as their influencing factors.

The production and concentration distribution of air pollutants are affected by many factors, and each air pollutant has a different source of pollution [4]. Among them, fossil fuel combustion, industrial production, transportation, and economic development heavily impact the generation and distribution of air pollutants [5–9]. Reducing pollutant emissions is key to improving air quality [10,11]. Given that the urban spatial structure

directly affects local meteorological conditions, such as urban temperature and ventilation, it also substantially impacts urban air quality [12–15]. The reported studies on influencing factors for urban air pollutants mainly use geographical detectors [16], multivariate Moran models [17], nonparametric panel models [5], and correlation analysis. The intensity and direction of air pollution are affected differently by the spatial structure of cities with different levels of size and economy [18]. Fan et al. [12] found that urban spatial structure impacted carbon emissions through transportation and environmental regulations. Zhang et al. [15,19] discussed the influence of urban spatial structure on PM_{2.5} concentration distribution and concluded that terrain elevation is an important factor affecting PM_{2.5} distribution. Miao et al. [14] observed that both urban green spaces and three-dimensional building patterns influenced the diffusion and transmission of air pollutants. Kan [13] speculated that the spatial structure of a boulevard significantly impacts the spatial distribution of the gaseous pollutants NO_x and SO₂. Another study concluded that urban sprawl will increase the local PM_{2.5} concentration [20]. Ding et al. [21] studied the microclimate environment by focusing on urban texture volume units and the urban external space environment comfort index. Fang and Qu [22] explored the correlation between urban spatial form and air quality and reported that urban form impacts air quality.

Regarding the impact of urban spatial structure on the urban environment (including air quality and thermal environments), determining the research scale and developing urban spatial structure indicators is an important research topic [23]. The framework and scale of urban heat island research have shifted from the “urban-suburban” dual structure to local climate zones (LCZ) [24]. Sapena et al. [25] extracted urban spatial structure indicators based on the LCZ classification framework and explored the relationship between urban spatial structure and the socioeconomic level of urban residents. Chen and Tang [26] studied the mapping method of local climate zoning and its application in planning simulations at different scales. Researchers have provided input to improve the application of LCZ in the field of urban planning in China [27–30]. Reportedly, greenery, enhancement of ground permeability, and rational adjustment of functional zoning can affect the comfort of the urban environment to varying degrees [31–33]. Most scholars have speculated that three-dimensional indicators have a greater impact on surface temperature than two-dimensional indicators, that the construction and selection of urban three-dimensional form indicators are insufficient, and that their guiding role in design and planning should be comprehensively considered [34–36].

In recent years, related research has mainly focused on the impact of urban spatial structure on the surface thermal environment. While the impact of urban spatial structure on urban air quality has not been extensively studied, the influence of urban spatial structure on urban gaseous pollutant concentration distribution is studied even less frequently. In addition, the current research mainly uses the relevant indicators of urban building distribution, such as floor area ratio, building density, sky openness, and other indicators, to study the impact of urban spatial structure on air quality, but the building height index is rarely used. In the current situation of more and more high-rise buildings in the city, it is a scientific issue worthy of attention to add height information on the basis of two-dimensional urban structure indicators and derive other spatial structure characteristics from height and two-dimensional indicators, so as to explore whether building height, volume, and dense distribution of buildings affect air quality. Based on the basic idea of local climate zoning, urban roads, Baidu building big data, and digital elevation model (DEM) data were used to divide the block and use it as the spatial scale in this study, such that the surface covering, building materials, and structures in the research unit were consistent. Using DEM data and building big data, an urban spatial structure index system was constructed based on three dimensions: one-dimensional height, two-dimensional plane, and three-dimensional space. Then, the spatial distribution pattern of gaseous pollutants (SO₂, NO₂, CO, and O₃) concentrations in Jinan City was obtained using interpolation methods such as ordinary kriging. Finally, correlation analysis, stepwise regression analysis, and bivariate global spatial autocorrelation analysis were used to explore the comprehensive

influence of urban spatial structure indicators on the concentration distribution of urban gaseous pollutants.

2. Materials and Methods

2.1. Study Area

Jinan, the capital of Shandong Province, is the province's political, economic, cultural, scientific, and educational center. Jinan has a warm, temperate monsoon climate with four distinct seasons. Summer is hot and humid; winter is cold and dry. Due to its inland location, the climate is more changeable under the influence of temperate continental and maritime climates. Jinan is located at the junction of the low hills in the middle and south of Shandong Province and the alluvial plain in the northwest of Shandong Province. Its topography is high in the south (Mount Tai) and low in the north (Yellow River). Surrounded by mountains, it is a bowl-shaped basin, which seriously hinders the operation and diffusion of air pollutants and easily causes the accumulation of air pollutants, which leads to frequent severe haze events in Jinan in summer and winter. The main sources of air pollutants are the burning of coal in the urban area of Jinan, the pollution emissions of heavy industry enterprises, the exhaust emissions of automobiles, and the exhaust emissions of diesel engines. The dust and the burning of biomass fuel in the rural areas around the city also emit a lot of pollutants into the air, which has caused a serious burden for the pollution control of Jinan. Shizhong, Huaiyin, Tianqiao, Licheng, and Lixia districts in Jinan City were chosen as the research area, which had a total area of approximately 2094 km². This region, where the buildings are the most densely distributed in Jinan City, experiences relatively heavy air pollution, which was favorable for exploring the influence of building distribution patterns on the distribution of air pollutants.

2.2. Data Source

The Jinan administrative boundary vector data used in this study were retrieved from the resource center of the Shandong geographic information public service platform <http://www.sdmap.gov.cn> (accessed on 6 August 2022). The DEM data, which have a spatial resolution of 9.08 m, were obtained from Google Earth. Baidu building big data of Jinan Central District were downloaded by Shuijingzhu map downloader. The data contains spatial information and attribute information such as building height and area. The road network data were downloaded by the Shuijingzhu map downloader, which contains the data of national roads, provincial roads, county roads, expressways, and urban first-class roads in the central urban area of Jinan City in 2020. The Landsat-8 remote sensing image data from the United States Geological Survey <https://earthexplorer.usgs.gov> (accessed on 6 August 2022), the image time was on 1 June 2017 and 7 June 2019, respectively, at 10:48 a.m. Beijing time, a total of four images, cloud cover is less than 5%, and the spatial resolution is 30 m. The air quality data for Jinan City were obtained from the ecological environment of Shandong Province's city ambient air quality monitoring data <http://sthi.shandonggov.cn/> (accessed on 6 August 2022). The above data were based on the administrative boundary data of Shandong Sky Map to perform geographic registration, spatial correction, and pre-processing such as projection transformation. The geographical coordinate system adopted CGCS2000, and the projection coordinate system adopted CGCS2000_3_Degree_GK_CM_117E. The scope of the study area and the distribution of its air quality stations are shown in Figure 1.

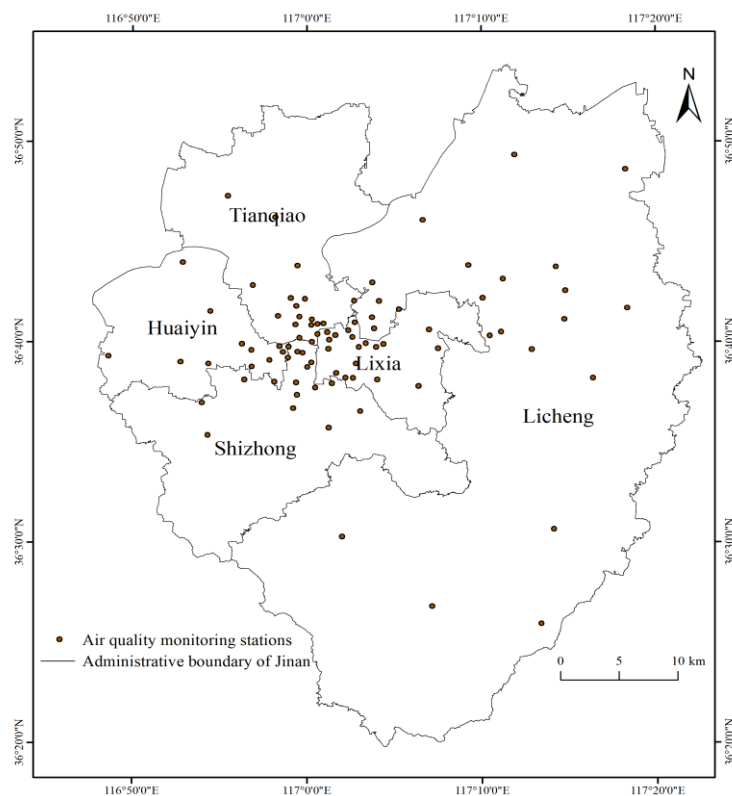


Figure 1. Distribution of air quality monitoring stations in the study area.

2.3. Research Method

2.3.1. Division of Research Units

In this study, we divided the research unit based on the actual distribution of buildings and roads in the central urban area of Jinan. There was a conscious effort to maintain consistency in the area, height, material, and other attributes of buildings in the same study unit. To this end, in the northern plain area of the city (where buildings and roads were more densely distributed), the urban road network was used to divide the study unit into neighborhoods. Moreover, for the southern low hills (where buildings and roads were sparse), DEM data were used to divide the area using the triangulated irregular network. The results of the preliminary division of neighborhoods were counted in terms of number and area size. The neighborhoods with too small an area were merged according to the principle of maximum side proximity, while the neighborhoods with too large an area were split according to the spatial distribution characteristics of buildings and surface cover to obtain the results of the final division of neighborhoods. The procedures and methods for dividing the neighborhood were as follows: (1) The merger of six types of roads: highways, urban primary roads, nine-level roads, county roads, provincial roads, and national roads were merged into the same layer to establish a vector road network for dividing the neighborhood. (2) Double-line roads were transformed into single-line roads by a closed mathematical morphology operation. First, the double-line roads were expanded, and a buffer zone of 80 m was established and merged according to the maximum width of the roads in Jinan. Then, the merged buffer was rasterized and binarized, after which a corrosion operation was carried out. Furthermore, the vectorization tool of the ArcScan toolbox (Arcmap 10.2) was used to extract the center line of the grid road, and the double-line road was transformed into a single-line road. (3) Road route elements were converted into surface elements. To process research units with an area less than 50,000 m², the adjacent surface with the longest common boundary was eliminated according to this principle, and the appropriate threshold was selected to eliminate the smaller research unit step by step. Larger research units with an area of more than 4 million m² were reasonably segmented according to the principle of consistent architectural attributes by comparing

building, road vector data, and high-definition images. The results of the divided research units are shown in Figure 2.

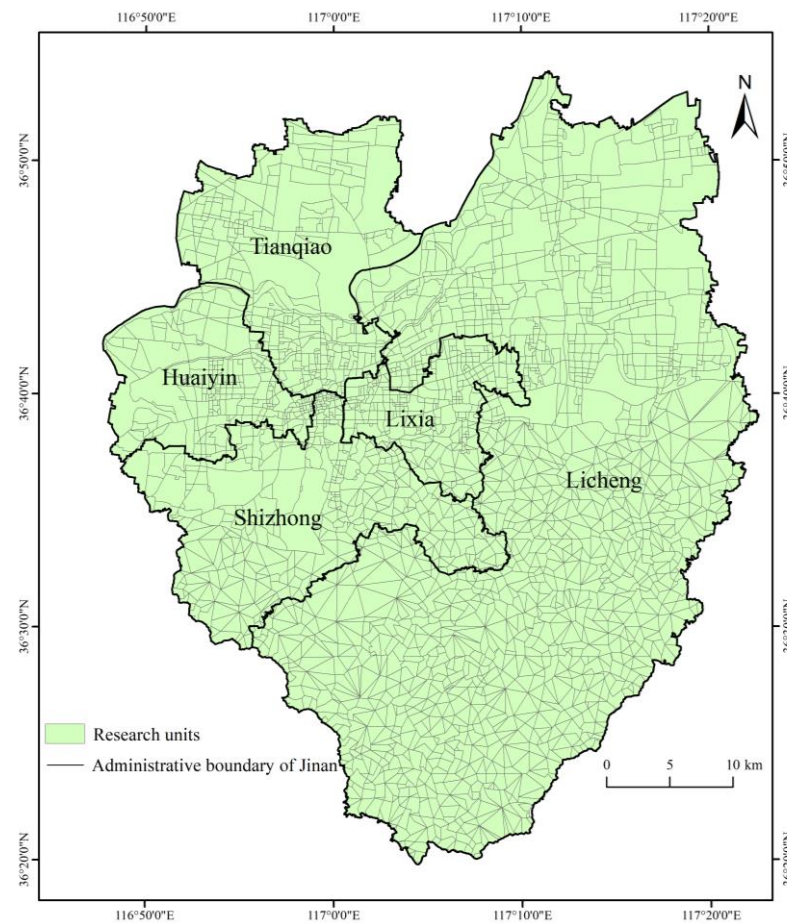


Figure 2. Division of research units in the study area.

2.3.2. Urban Spatial Structure Index System

Architecture is an important aspect of a city, and its spatial distribution directly affects the urban spatial structure. The studies of Zhang et al. and Chen et al., respectively, found that one-dimensional, two-dimensional, and three-dimensional urban spatial structure indicators have an impact on PM_{2.5} concentration and land surface temperature. Based on the reports by Chen et al. and Zhang et al. [23,37], this study determined the urban spatial structure index using building big data and DEM and constructed it with one-dimensional height, two-dimensional plane, and three-dimensional space.

The one-dimensional height index directly affects airflow, which influences urban air quality. Quantitative indicators in a two-dimensional plane characterize the area and plane characteristics of buildings in the study area. Quantitative indicators in three-dimensional space characterize the three-dimensional characteristics of buildings in the study area and influence air flow, thereby affecting air quality. Each index was calculated using the ArcGIS 10.2 grid calculator. The indexes and their meanings are listed in Table 1.

Table 1. Urban Spatial structure indexes and their meanings.

Quantitative Indexes	Meaning of the Indexes
DEM average height (H1)	Reflects the average high and low level of the terrain in the study area
DEM standard deviation (H2)	Reflects the severity of topographic changes in the study area
Maximum building height (H3)	Reflects the vertical height level of the tallest building in the study area
Average building height (H4)	Reflects the average level of vertical heights of buildings in the study area
Standard deviation of building height (H5)	Reflects the drastic changes in the vertical height of the buildings in the study area
Average building base area (S1)	Reflects the average level of building footprint in the study area
Total base area of the building (S2)	Reflects the overall situation of the land occupied by buildings in the study area
Standard deviation of building base area (S3)	Reflects the sharpness of the difference in the size of the buildings in the study area
Average building area (S4)	Reflects the average level of construction area in the study area
Total building area (S5)	Reflects the overall situation of the construction area in the study area
Standard deviation of building area (S6)	Reflects the drastic degree of difference in floor area within the study area
Building density (S7)	Reflects the density of buildings in the study area
Average building volume (V1)	Reflects the average building volume in the study area
Total building volume (V2)	Reflects the total building volume level in the study area
Standard deviation of building volume (V3)	Reflects the differences in the size of buildings in the study area
Volume rate (V4)	Reflects the efficiency and density of building land in the study area

2.3.3. Kriging Interpolation

By selecting the air quality data of Jinan City as the monitoring station data, kriging interpolation was utilized to obtain the spatial distribution data of SO₂, NO₂, CO, and O₃ concentrations in Jinan City. Kriging is a geostatistical method that generates the estimated surface through a set of dispersion points with Z-value. This method assumes that the distance or direction between the sampling points can reflect the spatial correlation of surface changes and uses a mathematical function that is fitted with a specified number of points or all points within a specified radius to determine the output value of each position. The measured values were weighted to obtain the predicted value Z(S₀) of the unmeasured position. This was calculated using Equation (1):

$$Z(S_0) = \sum_{i=1}^N \lambda_i Z(S_i) \tag{1}$$

where Z(S_i) is the measured value at position *i* (unit: µg/m³), *i* is the weight of the measured value at position *i*, S₀ is the predicted position, and *N* is the number of measured values.

The commonly used kriging methods are ordinary kriging, universal kriging, co-kriging, and disjunctive kriging. Different methods have their own applicable conditions; the optimal model can be determined through verification and cross-validation. The criterion of the optimal model is as follows: mean standardized error is closest to 0, root-mean-square prediction error is minimum, average mean error is closest to root-mean-square, and root-mean-square standardized prediction error is closest to 1.

2.3.4. Bivariate Global Spatial Autocorrelation Analysis

Bivariate global spatial autocorrelation analysis was proposed on the basis of the spatial autocorrelation index (Moran's I index), which aimed to solve the problem of spatial correlation of multiple variables. Bivariate global spatial autocorrelation analysis explores and analyzes the spatial correlation between multiple variables and can reveal the degree of correlation between one attribute of a spatial study unit and another attribute of a neighboring spatial study unit. The adjacency used in this study was the Queen connection, which calculated the spatial relationship between the central grid and the surrounding neighboring grids to generate a weight file. The bivariate global spatial autocorrelation was calculated, as shown in Equation (2):

$$I = \frac{\sum_{p=1}^n \sum_{q=1}^n Z_{pq} (x_p - \bar{x}) (y_q - \bar{y})}{S^2 \sum_{p=1}^n \sum_{q=1}^n Z_{pq}} \quad (2)$$

where I is the bivariate null global spatial autocorrelation coefficient between study units p and q , x_p denotes the attribute value of the independent variable of spatial unit p , and y_q denotes the attribute value of the dependent variable of spatial unit q . The mean values of the independent and dependent variables are as follows: S^2 is the variance of the variables, Z_{pq} is the spatial weight matrix between spatial units p and q established based on the Queen neighborhood relationship, x_p is the mean value of gaseous pollutant concentration within spatial cell p , and y_q is denoted as the attribute value of each urban spatial structure indicator within a spatial raster q . The bivariate spatial autocorrelation coefficient I is generally tested using the Z-value and its corresponding p -value. The spatial correlation of the two variables is generally significant when $|Z| \geq 1.96$. This method allowed for the exploration of the spatial correlation between the concentration of gaseous pollutants in each study unit and its surrounding regional urban spatial structure indicators.

3. Results and Discussion

3.1. Spatial Pattern of Gaseous Pollutants

The monitoring data of gaseous pollutants (NO_2 , SO_2 , CO , and O_3) from 76 stations in Jinan City in June and December 2020 were used to analyze the spatial distribution characteristics of gaseous pollutants using the Kriging spatial interpolation method. Furthermore, validation, cross-validation, and error comparison analyses were performed using ordinary kriging and simple kriging methods, as shown in Figure 3.

As shown in Figure 3, the high concentration area of NO_2 in Jinan during June was mainly in the northeastern part of the city, and the low concentration area was primarily located in the southern low hills with high vegetation cover, thus showing a decreasing trend from north to south. The NO_2 concentration in December was higher than that in June, and its concentration distribution was roughly similar to that in June. The high concentration area of SO_2 in June was mainly in the northeast, west-central, and east-central parts of the city, and the low concentration area was in the northwest and southwest parts of the city; the high concentration area in December was in the northernmost and south-central parts of the city, and the low concentration area was located in the central and southwest fringe areas of the city. The spatial distribution of SO_2 was irregular in June and December, with higher SO_2 concentrations in December than in June. The spatial distribution trends of CO concentrations were similar in June and December, with a stepwise decrease from northeast to southwest and a higher CO concentration in December than in June. The low O_3 concentration area in June was distributed in the central, western, and southernmost parts of the city, and the distribution trend decreased from east to west. The high O_3 concentration area in December was mainly distributed in the southern mountainous area, and the low concentration area was in the northern part of the city; the distribution trend increased from north to south. The distribution of O_3 concentration in June was higher

than that in December, mainly because of the high light intensity and high temperature in the summer.

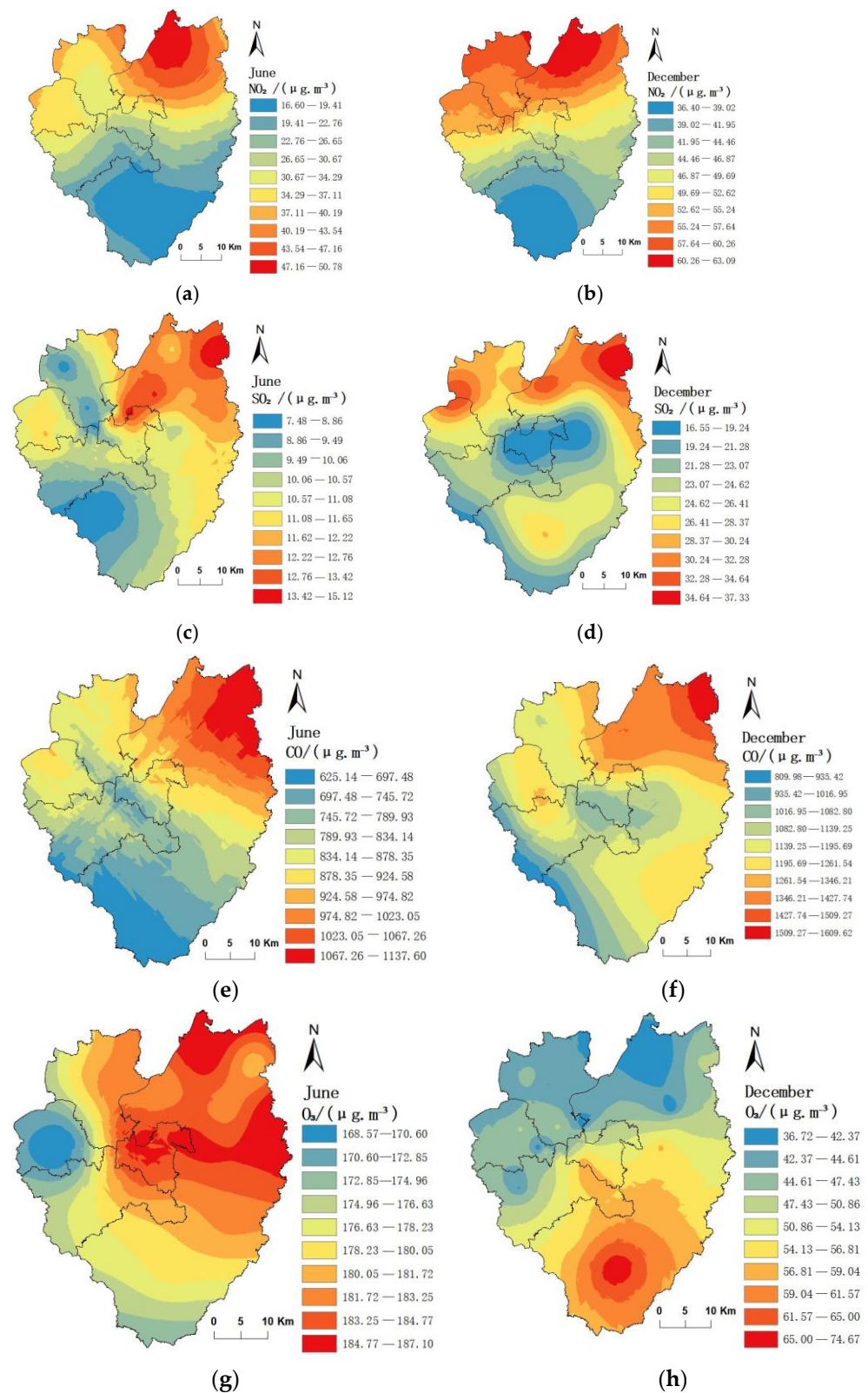


Figure 3. Spatial distribution of NO_2 , SO_2 , CO , and O_3 concentrations in Jinan in 2020. (a) NO_2 concentrations in June. (b) NO_2 concentrations in December. (c) SO_2 concentrations in June. (d) SO_2 concentrations in December. (e) CO concentrations in June. (f) CO concentrations in December. (g) O_3 concentrations in June. (h) O_3 concentrations in December.

Overall, air quality was better in the southern part of the city than in the northern part, with NO₂, SO₂, and CO (except O₃) concentrations higher in December than in June. This was due to the large difference between the spatial structure of the southern mountainous area and the northern urban area. The population density and building density in the south were smaller than those in the north, which produced fewer pollutants and had strong air mobility. The high forest cover in the southern mountainous area had strong air purification capacity. By contrast, high temperatures in June, strong solar radiation, lush vegetation growth, frequent monsoons, high wind speeds, and accelerated air convection resulted in an unstable boundary layer of pollutants and heavy rainfall, which were conducive to the diffusion and degradation of pollutants; low temperatures and dry conditions with little rain in December increased the demand for heating and gas. Vegetation withered and weakened the ability to purify the air, leading to poor diffusion conditions and an increase in the concentration of pollutants. High temperatures, strong light, and sunny weather in June resulted in an increase in the amount of radiation reaching the ground, thereby producing more O₃. Thus, the O₃ concentration in December was lower than that in June.

3.2. Correlation Analysis between Gaseous Pollutant Distribution and Urban Spatial Structure Indicators

The Pearson correlation coefficients of gaseous pollutant (SO₂, NO₂, CO, and O₃) concentrations and urban spatial structure indicators in Jinan were calculated using the Corrcof function of MATLAB R2014b in June and December and tested for significance. The results are shown in Tables 2 and 3.

Table 2. The correlation coefficient between gaseous pollutant concentrations and urban spatial structure indexes in June.

Urban Spatial Structure Indexes	NO ₂	SO ₂	CO	O ₃
H1	−0.6390 ***	−0.0278	−0.2043 ***	0.1396 ***
H2	−0.5731 ***	−0.0684 *	−0.2242 ***	0.0910 **
H3	−0.0436	−0.0010	−0.1122 ***	0.0186
H4	−0.0509	0.0393	0.0343	−0.0088
H5	−0.0051	0.0506	0.0027	0.0009
S1	0.0200	0.0327	0.0651 *	−0.0067
S2	−0.0297	−0.0315	−0.1084 ***	0.0257
S3	0.0114	−0.0139	−0.0146	−0.0061
S4	0.0200	0.0327	0.0651 *	−0.0067
S5	−0.0297	−0.0315	−0.1084 ***	0.0257
S6	0.0114	−0.0139	−0.0146	−0.0061
S7	−0.6426 ***	−0.0276	−0.2437 ***	0.1440 ***
V1	−0.6352 ***	−0.0214	−0.1955 ***	0.1358 ***
V2	−0.0051	0.0506	0.0027	0.0009
V3	−0.0224	−0.2488 ***	−0.3174 ***	0.0342
V4	−0.0760 *	−0.1998 ***	−0.2956 ***	0.0598

Note: *** indicates that the correlation reached a significance level of 0.001; ** indicates that it reached a significance level of 0.01; * indicates that it reached a significance level of 0.05.

As can be seen from Tables 2 and 3, in June, the NO₂ concentration was negatively correlated with H1, H2, S7, V1, and V4. It reached a significance level of 0.001 with H1, H2, S7, and V1. In December, NO₂ concentration was negatively correlated with H1, H2, and H4 and reached a significance level of 0.001, and NO₂ concentration was positively correlated with S1, S2, S3, S5, S7, V2, and V4, where it reached a significance level of 0.001 with S1, S2, S3, S7, and V4. The NO₂ concentrations in June and December were correlated with H1, H2, S7, and V4, and the correlation among H1, H2, and S7 for NO₂ concentration was significant, reaching a significance level of 0.001. This indicated that the topographic

elevation of Jinan City and its degree of undulation and building density are important influencing factors for the distribution of NO₂ concentration.

Table 3. The correlation coefficient between gaseous pollutant concentrations and urban spatial structure indexes in December.

Urban Spatial Structure Indexes	NO ₂	SO ₂	CO	O ₃
H1	−0.8106 ***	−0.2717 ***	−0.3300 ***	0.7671 ***
H2	−0.6933 ***	−0.1878 ***	−0.2961 ***	0.6490 ***
H3	0.0476	−0.2889 ***	−0.1433 ***	0.0173
H4	−0.1142 ***	−0.2376 ***	−0.1549 ***	0.1766 ***
H5	−0.0223	−0.2751 ***	−0.1251 ***	0.0910 **
S1	0.1130 ***	0.0067	0.0279	−0.0775 *
S2	0.1649 ***	0.0393	0.0723 *	−0.1880 ***
S3	0.1226 ***	0.0465	0.0651 *	−0.0948 **
S4	−0.0300	−0.1649 ***	−0.0920 **	0.0890 **
S5	0.0763 *	−0.1126 ***	−0.0409	−0.0763 *
S6	0.0461	−0.1512 ***	−0.0894 **	0.0110
S7	0.3476 ***	−0.1365 ***	−0.1165 ***	−0.2597 ***
V1	−0.0300	−0.1649 ***	−0.0920 **	0.0890 **
V2	0.0763 *	−0.1126 ***	−0.0409	−0.0763 *
V3	0.0461	−0.1512 ***	−0.0894 **	0.0110
V4	0.2013 ***	−0.2921 ***	−0.2127 ***	−0.0958 **

Note: The meaning of ***, **, * is the same as in Table 2.

In June, SO₂ concentration was negatively correlated with H2, V3, and V4, and V3 and V4 reached a significance level of 0.001. All other indicators had no significant effect on SO₂ concentration. All indicators, except S1, S2, and S3, were negatively correlated with SO₂ concentration in December and reached a significance level of 0.001. SO₂ concentrations in both June and December were correlated with H2, V3, and V4 and reached a significance level of 0.001 in the case of V3 and V4. This indicated that topographic relief, building volume standard deviation, and volume ratio had significant effects on SO₂ concentration distribution.

In June, the CO concentration was positively correlated with S1 and S4, reaching a significance level of 0.05. It was negatively correlated with H1, H2, H3, S2, S5, S7, V1, V3, and V4, reaching a significance level of 0.001. In December, the CO concentration was positively correlated with S2 and S3, reaching a significance level of 0.05. It was negatively correlated with H1, H2, H3, H4, H5, S4, S6, S7, V1, V3, and V4, where the correlation with H1, H2, H3, H4, H5, S7, and V4 reached a significance level of 0.001, and the correlation with S4, S6, V1, and V3 reached a significance level of 0.01. The CO concentrations in both June and December were correlated with H1, H2, H3, S2, S4, S7, V1, V3, and V4. The negative correlation between H1, H2, H3, S7, and V4 and the CO concentrations in June and December reached a significance level of 0.001, indicating that the CO concentration was influenced majorly by topographic elevation, degree of undulation, building density, and volume ratio.

In June, the O₃ concentration was positively correlated with H1, H2, S7, and V1, with S7 and V1 attaining a significance level of 0.001. The correlations of other indicators were not significant, indicating that O₃ concentrations were strongly correlated with topographic elevation, building density, and average building volume. In December, O₃ concentrations were positively correlated with H1, H2, H4, H5, S4, and V1, with correlations reaching a significance level of 0.001 with H1, H2, and H4 and 0.01 with H5, S4, and V1. Moreover, O₃ concentrations were negatively correlated with S1, S2, S3, S5, S7, V2, and V4, with correlations reaching a significance level of 0.001 with S2 and S7, 0.01 with S3, and 0.5 with S1, S5, V2, and V4. This indicated that O₃ concentration was mainly influenced by topographic elevation (H1, H2, and H4), building total basal area (S2), and building density

(S7). In June and December, H1, S7, and V1 had significant effects on O₃ concentrations, reaching a significance level of 0.01. This revealed that indicators such as topographic elevation, building density, and average building volume had significant effects on the spatial distribution of O₃ concentrations.

The concentration of gaseous pollutants showed obvious seasonal characteristics, and the urban spatial structure index that affected the concentration of gaseous pollutants also showed seasonal characteristics. In summer (such as June), the concentration of NO₂, CO, and SO₂ is the lowest, and there are fewer urban spatial structure indicators with significant correlation with them; in winter (such as December), the concentration of NO₂, CO, and SO₂ is the highest, and there are more urban structural spatial indicators with significant correlation with them. In the spring and autumn months, the concentration of gaseous pollutants is in the middle. The seasonal distribution characteristics of O₃ concentration are opposite to those of NO₂, CO, and SO₂ concentration. NO₂, CO, and O₃ concentrations were related to topographic elevation and building density; SO₂ and CO concentrations were related to the volume ratio. Given that the terrain of Jinan is high around and low in the middle, pollutants accumulated at low-lying places and did not dissipate easily to higher-elevation regions. In addition, the higher the building density and floor area ratio, the more concentrated the population, and the greater the corresponding degree of increase in traffic activities, energy consumption, and fuel consumption. Thus, pollutants emitted by humans were concentrated in that spatial area.

3.3. Stepwise Regression Analysis of Gaseous Pollutant Distribution and Urban Spatial Structure Indexes

To further analyze the influence of urban spatial structure indicators on the spatial distribution of air gaseous pollutant concentrations, a stepwise regression analysis of gaseous pollutant concentrations on urban spatial structure indicators was conducted using the stepwise function of MATLAB R2014b. The results of the stepwise regression analysis are shown in Tables 4 and 5.

Table 4. Results of stepwise regression analysis of gaseous pollutant concentrations and urban spatial structure indexes in June.

Pollutants	Formulas	Test Values
NO ₂	$Y = x_2 \times (-8.88 \times 10^{-5}) + x_3 \times (2.87 \times 10^{-5}) + x_{10} \times (-5.84 \times 10^{-10}) + x_{12} \times (-3.42 \times 10^{-5}) + x_{15} \times (-0.0147) + 0.0393$	$R^2 = 0.5208$ $Adj R^2 = 0.5179$ $F = 175.73$ $P = 3.46 \times 10^{-151}$
SO ₂	$Y = x_2 \times (-3.48 \times 10^{-5}) + x_{12} \times (2.52 \times 10^{-6}) + x_{15} \times (-0.0029) + x_{16} \times (-0.0001) + 0.01141$	$R^2 = 0.1172$ $Adj R^2 = 0.1127$ $F = 25.78$ $P = 1.72 \times 10^{-24}$
CO	$Y = x_2 \times (-0.0028) + x_6 \times (2.48 \times 10^{-6}) + x_{15} \times (-0.2193) + x_{16} \times (-0.0227) + 0.9280$	$R^2 = 0.2899$ $Adj R^2 = 0.2863$ $F = 79.30$ $P = 8.10 \times 10^{-70}$
O ₃	$Y = x_{12} \times (9.07 \times 10^{-6}) + x_{15} \times (0.0031) + 0.1792$	$R^2 = 0.0269$ $Adj R^2 = 0.0249$ $F = 13.47$ $P = 1.69 \times 10^{-6}$

Table 5. Results of stepwise regression analysis of gaseous pollutant concentrations and urban spatial structure indexes in December.

Pollutants	Formulas	Test Values
NO ₂	$Y = x1 \times (-1.26 \times 10^{-5}) + x13 \times (-2.28 \times 10^{-5}) + 0.0563$	R ² = 0.6635 Adj R ² = 0.6628 F = 960.16 P = 4.52 × 10 ⁻²³¹
SO ₂	$Y = x12 \times (-1.58 \times 10^{-5}) + x16 \times (-0.0012) + 0.0261$	R ² = 0.2399 Adj R ² = 0.2383 F = 153.67 P = 9.90 × 10 ⁻⁵⁹
CO	$Y = x2 \times (-0.0015) + x10 \times (-1.86 \times 10^{-8}) + x12 \times (-0.0002) + x15 \times (-0.2397) + 1.2678$	R ² = 0.2422 Adj R ² = 0.2383 F = 62.06 P = 3.28 × 10 ⁻⁵⁶
O ₃	$Y = x3 \times (8.50 \times 10^{-6}) + x7 \times (1.83 \times 10^{-9}) + x13 \times (3.86 \times 10^{-5}) + x15 \times (0.0059) + x16 \times (0.0006) + 0.0440$	R ² = 0.6235 Adj R ² = 0.6212 F = 267.71 P = 8.25 × 10 ⁻²⁰²

As can be seen from Tables 4 and 5, the p-values of the stepwise regression equation tests of gaseous pollutant concentrations and urban spatial structure indicators in June and December were close to zero, reaching a very high level of significance.

In June, NO₂ concentration regressed well with H2, H3, S5, S7, and V3, where it was positively correlated with H3 and NO₂ concentration and negatively correlated with H2, S5, S7, and V3 concentration. The regression of SO₂ concentration with H2, S7, V3, and V4 was good and was positively correlated with S7 and negatively correlated with H2, V3, and V4. The regressions of CO concentration with H2, S1, V3, and V4 were good, showing positive correlation with S1 and negative correlation with H2, V3, and V4. The regressions of O₃ concentrations with S7 and V3 were good and positively correlated.

In December, the regression of NO₂ concentration using H1 and V1 of DEM was good and negatively correlated. The regression of SO₂ concentration using S7 and V4 was good and negatively correlated. The regressions of CO concentration and H2, S5, S7, and V3 were good and negatively correlated. The regressions of O₃ concentration with H3, S2, V1, V3, and V4 were good and positively correlated.

3.4. Bivariate Global Spatial Autocorrelation Analysis of Gaseous Pollutant Distribution and Urban Spatial Structure Indicators

The influence of urban spatial structure indicators of the surrounding areas on the concentration distribution of gaseous pollutants, using gaseous pollutant concentration as the first variable and urban spatial structure indicators as the second variable, needed to be analyzed. To this end, a first-order posterior adjacency matrix (Queen) was selected using the GeoDa software to establish a spatial weight file, calculate the global Moran’s I value and its test value Z-value between the two variables, and explore the spatial correlation between the gaseous pollutant concentration and its surrounding regional urban spatial structure indicators (Tables 6 and 7).

As can be seen from Table 6, the |Z| values of the bivariate Moran’s I test for NO₂, CO, and O₃ concentrations and all urban spatial structure indicators were greater than 1.96 in June, indicating that all urban spatial structure indicators in the surrounding area had a significant effect on the concentration distribution of the three gaseous pollutants in the region. Among them, the spatial correlation between NO₂ concentration and H3, H4, H5, S2, S3, S6, S7, and V3 in the adjacent regions was greater; the spatial correlation between CO concentration and H3, H4, H5, S1, S3, S6, and V3 in the adjacent regions was greater; and the spatial correlation between O₃ concentration and H3, H4, H5, S2, S5, S6, S7, V2, V3,

and V4 in the adjacent regions was greater. The spatial correlation of SO₂ concentration with S4 and V1 was not significant, whereas the spatial correlations with other urban spatial structure indicators were significant. The spatial correlation between SO₂ concentration and H4, H5, S1, S3, S6, and V3 in the adjacent area was more pronounced. The spatial correlation of NO₂, SO₂, CO, and O₃ concentrations with H1 and H2 was negative, while the spatial correlation with other urban spatial structure indicators was positive.

Table 6. Results of bivariate global spatial autocorrelation analysis of gaseous pollutant concentrations and urban spatial structure indexes in June.

	NO ₂		SO ₂		CO		O ₃	
	Moran's I	Z	Moran's I	Z	Moran's I	Z	Moran's I	Z
H1	−0.794	−61.67	−0.417	−37.62	−0.592	−49.86	−0.148	−13.61
H2	−0.794	−63.62	−0.436	−39.03	−0.652	−56.02	−0.168	−16.14
H3	0.262	24.94	0.033	3.19	0.18	17.14	0.185	17.51
H4	0.259	24.54	0.085	8.30	0.199	18.66	0.207	19.33
H5	0.236	22.51	0.054	5.25	0.166	15.71	0.161	15.14
S1	0.194	19.08	0.059	5.87	0.148	14.38	0.08	6.99
S2	0.228	22.22	−0.044	−4.32	0.123	12.02	0.162	15.97
S3	0.215	20.81	0.08	7.79	0.159	15.38	0.071	7.11
S4	0.091	8.73	0.001	0.13	0.071	6.74	0.045	3.75
S5	0.197	19.75	−0.08	−7.93	0.109	10.93	0.19	18.69
S6	0.21	19.88	0.052	4.99	0.141	13.27	0.11	10.74
S7	0.207	19.95	−0.065	−6.23	0.098	9.35	0.132	12.77
V1	0.091	8.73	0.001	0.13	0.071	6.74	0.045	3.75
V2	0.197	20.20	−0.08	−7.93	0.109	10.93	0.19	18.69
V3	0.21	19.88	0.052	4.99	1.041	13.27	0.11	10.74
V4	0.183	18.05	−0.06	−5.79	0.093	9.08	0.172	16.90

Table 7. Results of bivariate global spatial autocorrelation analysis of gaseous pollutant concentrations and urban spatial structure indexes in December.

	NO ₂		SO ₂		CO		O ₃	
	Moran's I	Z	Moran's I	Z	Moran's I	Z	Moran's I	Z
H1	−0.795	−60.88	−0.88	−8.46	−0.36	−32.89	−0.331	−30.58
H2	−0.779	−61.70	−0.136	−13.31	−0.378	−34.28	−0.331	−31.26
H3	0.171	16.47	0.112	11.15	−0.014	−1.36	−0.267	−24.89
H4	0.186	17.54	0.072	7.19	0.053	5.16	−0.195	−18.60
H5	0.156	15.09	0.08	7.94	0.017	1.60	−0.238	−22.19
S1	0.148	14.46	0.06	5.70	0.034	3.35	−0.115	−11.26
S2	0.152	14.55	0.124	11.89	0.092	−9.04	−0.247	−23.32
S3	0.172	16.54	0.044	4.24	0.053	5.14	−0.105	−10.08
S4	0.059	5.74	0.05	4.88	−0.015	−1.56	−0.104	−10.08
S5	0.108	10.68	0.151	14.80	−0.122	−12.05	−0.281	−26.56
S6	0.153	14.39	0.046	4.54	0.018	1.72	−0.183	−17.50
S7	0.139	13.32	0.127	12.42	−0.12	−11.50	0.232	−21.60
V1	0.059	5.74	0.05	4.88	−0.015	−1.56	−0.104	−10.08
V2	0.108	10.68	0.151	14.80	−0.122	−12.05	−0.281	−26.56
V3	0.153	14.39	0.046	4.54	0.018	1.72	−0.183	−17.50
V4	0.109	10.66	0.12	12.10	−0.106	−10.22	−0.247	−23.23

As seen in Table 7, the |Z| value of the bivariate Moran's I test for NO₂, SO₂, and O₃ concentrations with all urban spatial structure indicators was greater than 1.96 in December, indicating that all urban spatial structure indicators in the surrounding area had a significant effect on the concentration distribution of these three gaseous pollutants in the region. Among them, NO₂ concentration showed a negative spatial correlation with H1 and H2 in the adjacent regions, a positive correlation with the rest of the indicators at different

degrees, and a greater spatial correlation with H3, H4, H5, S2, S3, S6, and V3 in the adjacent regions. The SO₂ concentration showed a significant negative spatial correlation with H1 and H2 in the adjacent regions and a greater spatial correlation with H3, S2, S5, S7, V2, and V4 in the adjacent regions. The negative spatial correlation between O₃ concentration and H1, H2, H3, H5, S2, S5, V2, and V4 in the adjacent area was highly significant, and O₃ concentration demonstrated a significant positive spatial correlation with only S7 in the adjacent area. The negative spatial correlation of CO concentration with H1, H2, S5, S7, V2, and V4 in the adjacent regions was significant; the positive spatial correlation with H4, S2, and S3 in the adjacent regions was significant. The spatial correlation with H3, H5, S4, S6, V1, and V3 was not significant.

4. Conclusions

Following are the major conclusions of the current study:

1. There were evident spatial and temporal differences in the concentration and distribution of gaseous pollutants in the central city of Jinan. Overall, NO₂, SO₂, and CO concentrations were higher in December than in June, and O₃ concentrations were higher and more differential in June than in December. Moreover, the distribution of NO₂ and CO concentrations showed spatial regularity, and pronounced spatial heterogeneity existed in the distribution of SO₂ and O₃ concentrations. The high concentration areas of NO₂ were mainly in the northeast region of the city, and the low concentration areas were in the southern low hills that had high vegetation coverage. Thus, a decreasing trend was observed from north to south, and the distribution was opposite to the distribution characteristics of the topographic elevation of Jinan; the CO concentration decreased in a stepwise manner from northeast to southwest.
2. Indicators, such as topographic elevation, building density, building volume, and volume ratio, were important factors affecting the distribution of gaseous pollutant concentrations. The reason may be that topographic elevation plays an important role in air flow and diffusion. In valleys or low-lying areas, due to the blocking effect of terrain, air is often unable to flow smoothly, resulting in the accumulation of gaseous pollutants in the area, which increases the concentration. On the contrary, in the mountains or highlands, the air flow is relatively smooth, which is conducive to the dilution and diffusion of pollutants, so that the concentration is reduced. Secondly, high building density is usually accompanied by higher population activities and energy consumption, which will increase the emission of pollutants but also limit the air flow and the space for the diffusion of pollutants, resulting in higher concentrations. In addition, the high building volume and floor area ratio mean that the distribution of buildings in the vertical direction is more concentrated, which may lead to the bottom space being limited, air flow blocked, pollutants accumulating at a lower height, and the concentration increasing. The lower building volume and floor area ratio contribute to better air circulation, allowing pollutants to be diluted and dispersed and the concentration to be reduced. Among these, the spatial distribution of NO₂ concentration was mainly influenced by terrain elevation and building density; the spatial distribution of SO₂ concentration was influenced by terrain undulation, building volume standard deviation, and volume ratio; the spatial distribution of CO concentration was significantly influenced by terrain elevation and its undulation degree, building density, and volume ratio; and the spatial distribution of O₃ concentration was determined by terrain elevation, building density, average building volume, and other indicators. Understanding and considering these factors and formulating appropriate measures in urban planning and environmental management can contribute to reducing pollutant emissions and improving air quality.
3. The combined effects of urban spatial structure indicators on the spatial distribution of gaseous pollutant concentrations varied over time; in June and December, meteorological conditions, such as temperature, humidity, wind speed, wind direction, and air pressure, as well as the distribution of gaseous pollutants in Jinan City, were

significantly different. The combined effects of one-dimensional, two-dimensional, and three-dimensional indicators of urban spatial structure on the dispersion and concentration distribution of gaseous pollutants were remarkably different. In general, the degree of topographic elevation undulation, building density, building volume standard deviation, volume ratio, and other indicators had a greater comprehensive impact on the spatial distribution of gaseous pollutant concentrations; the more undulating the topography, the denser the distribution of buildings, and the larger the volume ratio. This increased the likelihood of air flow obstruction in the region, thereby affecting the diffusion and distribution of gaseous pollutants.

4. The urban spatial structure indicators of the surrounding areas had a remarkable influence on the spatial distribution of gaseous pollutant concentrations. The concentrations of NO₂, SO₂, CO, and O₃ showed significant negative spatial correlations with DEM average height and DEM standard deviation in the adjacent areas. In June, the concentrations of gaseous pollutants showed a significant positive spatial correlation with building mean height, building height standard deviation, building area standard deviation, and building density in the adjacent areas.

Author Contributions: B.S.: Conceptualization, data curation, resources, formal analysis, methodology, funding acquisition, writing components of original draft, review, and editing. Q.R.: Conceptualization, data curation, methodology, visualization, writing components of original draft, review, and editing. Q.Z.: visualization, writing—review and editing. C.S.: data curation, writing—review and editing. All authors have read and agreed to the published version of the manuscript.

Funding: This work was financially supported by the Humanities and Social Science Fund of the Ministry of Education of the People's Republic of China (No. 12YJA790019) and the National Natural Science Foundation of China (No. 51608309).

Institutional Review Board Statement: Not applicable.

Informed Consent Statement: Not applicable.

Data Availability Statement: The Jinan administrative boundary vector data used in this study were retrieved from the resource center of the Shandong geographic information public service platform <http://www.sdmap.gov.cn> (accessed on 6 August 2022). The Landsat-8 remote sensing image data from the United States Geological Survey <https://earthexplorer.usgs.gov> (accessed on 6 August 2022). The air quality data for Jinan City were obtained from the ecological environment of Shandong Province's city ambient air quality monitoring data <http://sthi.shandonggov.cn/> (accessed on 6 August 2022).

Conflicts of Interest: The authors declare no conflict of interest.

References

1. Loaiza-Ceballos, M.C.; Marin-Palma, D.; Zapata, W.; Hernandez, J.C. Viral respiratory infections and air pollutants. *Air Qual. Atmos. Health* **2021**, *5*, 105–114. [[CrossRef](#)]
2. Shahriyari, H.A.; Nikmanesh, Y.; Jalali, S.; Tahery, N.; Fard, A.Z.; Hatamzadeh, N.; Zarea, K.; Cheraghi, M.; Mohammadi, M.J. Air pollution and human health risks: Mechanisms and clinical manifestations of cardiovascular and respiratory diseases. *Toxin Rev.* **2022**, *41*, 606–617. [[CrossRef](#)]
3. Fahed, J.; Kinab, E.; Ginetet, S.; Adolphe, L. Impact of urban heat island mitigation measures on microclimate and pedestrian comfort in a dense urban district of Lebanon. *Sustain. Cities Soc.* **2020**, *61*, 102375. [[CrossRef](#)]
4. Jiang, P.; Chen, X.; Li, Q.; Mo, H.; Li, L. High-resolution emission inventory of gaseous and particulate pollutants in Shandong Province, eastern China. *J. Clean. Prod.* **2020**, *259*, 120806. [[CrossRef](#)]
5. Liu, D.; He, Y.; Wang, Q. Urban spatial structure evolution and smog management in China: A re-examination using nonparametric panel model. *J. Clean. Prod.* **2021**, *285*, 124847. [[CrossRef](#)]
6. Lu, Y.; Shao, M.; Zheng, C.; Ji, H.; Gao, X.; Wang, Q. Air pollutant emissions from fossil fuel consumption in China: Current status and future predictions. *Atmos. Environ.* **2020**, *231*, 117536. [[CrossRef](#)]
7. Tsai, I.-C.; Lee, C.-Y.; Lung, S.-C.C.; Su, C.-W. Characterization of the vehicle emissions in the Greater Taipei Area through vision-based traffic analysis system and its impacts on urban air quality. *Sci. Total Environ.* **2021**, *782*, 146571. [[CrossRef](#)] [[PubMed](#)]
8. Xiao, C.; Chang, M.; Guo, P.; Gu, M.; Li, Y. Analysis of air quality characteristics of Beijing–Tianjin–Hebei and its surrounding air pollution transport channel cities in China. *J. Environ. Sci.* **2020**, *87*, 213–227. [[CrossRef](#)]

9. Zhao, C.; Sun, Y.; Zhong, Y.; Xu, S.; He, M. Spatio-temporal analysis of urban air pollutants throughout China during 2014–2019. *Air Qual. Atmos. Health* **2021**, *14*, 1619–1632. [[CrossRef](#)]
10. Song, Y.; Li, Z.; Liu, J.; Yang, T.; Zhang, M.; Pang, J. The effect of environmental regulation on air quality in China: A natural experiment during the COVID-19 pandemic. *Atmos. Pollut. Res.* **2021**, *12*, 21–30. [[CrossRef](#)]
11. Zhao, X.; Shen, N.; Li, L.; Wu, G.; Tao, J.; Zhao, W. Analysis of Changes and Factors Influencing Air Pollutants in the Beijing-Tianjin-Hebei Region During the COVID-19. *Environ. Sci.* **2021**, *42*, 1205–1214. [[CrossRef](#)]
12. Fan, Q.; Wang, J.; Wang, J. The Emission Reduction Effect of Urban Spatial Structure Evolution: Internal Mechanism and Chinese Experience. *Urban Issues* **2021**, *12*, 87–96. [[CrossRef](#)]
13. Kan, L. Influence of Boulevard Spatial Structures on Distribution Characteristics of NO_x and SO₂ in Urban Shanghai City. *Res. Environ. Sci.* **2020**, *33*, 18–26. [[CrossRef](#)]
14. Miao, C.; He, H.; Chen, W.; Hu, Y.; Liu, M. Research progress on the influence of urban green space and three-dimensional building pattern on air pollutants. *Chin. J. Ecol.* **2021**, *8*, 1–7, preprint. [[CrossRef](#)]
15. Zhang, Z.; Shan, B.; Lin, Q.; Chen, Y.; Yu, X.; Zhu, M. Influence of urban spatial structure on PM_{2.5} concentration distribution. *Environ. Eng.* **2021**, *39*, 84–91. [[CrossRef](#)]
16. Wu, H.S.; Hong, S.; Hu, M.G.; Li, Y.H.; Yun, W.Z. Assessment of the Factors Influencing Sulfur Dioxide Emissions in Shandong, China. *Atmosphere* **2022**, *13*, 142. [[CrossRef](#)]
17. Yao, Y.R.; He, C.; Li, S.Y.; Ma, W.C.; Li, S.; Yu, Q.; Mi, N.; Yu, J.; Wang, W.; Yin, L.; et al. Properties of particulate matter and gaseous pollutants in Shandong, China: Daily fluctuation, influencing factors, and spatiotemporal distribution. *Sci. Total Environ.* **2019**, *660*, 384–394. [[CrossRef](#)]
18. Wang, F.; Dong, M.R.; Ren, J.; Luo, S.; Zhao, H.; Liu, J. The impact of urban spatial structure on air pollution: Empirical evidence from China. *Environ. Dev. Sustain.* **2022**, *24*, 5531–5550. [[CrossRef](#)]
19. Zhang, Z.; Shan, B.; Lin, Q.; Chen, Y.; Yu, X. Influence of the spatial distribution pattern of buildings on the distribution of PM_{2.5} concentration. *Stoch. Environ. Res. Risk Assess.* **2021**, *36*, 985–997. [[CrossRef](#)]
20. Qin, M.; Liu, X.; Tong, Y. Does Urban Sprawl Exacerbate Haze Pollution—An Empirical Study of Fine Particles (PM_{2.5}) in Chinese Cities. *Financ. Trade Econ.* **2016**, *37*, 15. [[CrossRef](#)]
21. Ding, W.; Hu, Y.; Dou, P. Research on the relationship between urban form and urban microclimate. *Archit. J.* **2012**, *6*, 16–21. [[CrossRef](#)]
22. Fang, Y.; Qu, L. Study on the Correlation between Urban Form and Air Quality. *Urban Construction* **2018**, *8*, 88–94. [[CrossRef](#)]
23. Shan, B.; Zhang, Q.; Ren, Q.; Fan, W.; Lu, Y. Spatial differentiation of urban thermal environment and its influencing factors based on local climate zones in Jinan. *J. Geo Inf. Sci.* **2022**, *24*, 711–722. [[CrossRef](#)]
24. Stewart, I.D.; Oke, T.R. Local climate zones for urban temperature studies. *Bull. Am. Meteorol. Soc.* **2012**, *93*, 1879–1900. [[CrossRef](#)]
25. Sapena, M.; Wurm, M.; Taubenböck, H.; Tuia, D.; Ruiz, L.A. Estimating quality of life dimensions from urban spatial pattern metrics. *Comput. Environ. Urban Syst.* **2021**, *85*, 101549. [[CrossRef](#)]
26. Chen, K.; Tang, Y. Research Progress of Local Climate Zones and Its Applications in Urban Planning. *South Archit.* **2017**, *2*, 21–28. [[CrossRef](#)]
27. Fang, B.; Ge, Y. The Evolution of Block Patterns and the Discussion on the Appropriate Scale of Block in the Development Course of Block System. *Urban Dev. Stud.* **2019**, *26*, 34–40. [[CrossRef](#)]
28. Liu, L.; Liu, J.; Lin, Y.; Wang, D. Local Climatic Analysis of Multiple Urban Surface Morphology. *Build. Sci.* **2017**, *33*, 8. [[CrossRef](#)]
29. Xiang, Y.; Zhang, Y.; Shi, Y. Study on Local Climate Zone Mapping in Highly Spatially Heterogeneous City. *Build. Sci.* **2020**, *36*, 9. [[CrossRef](#)]
30. Xu, H.; Yu, B.; Chen, G.; Liu, Y.; Pu, Y. Urban block extraction and accuracy evaluation based on Open Street Map data. *Geospat. Inf.* **2019**, *17*, 5. [[CrossRef](#)]
31. Coseo, P.; Larsen, L. How factors of land use/land cover, building configuration, and adjacent heat sources and sinks explain Urban Heat Islands in Chicago. *Landsc. Urban Plan.* **2014**, *125*, 117–129. [[CrossRef](#)]
32. Peng, F.; Wong, M.S.; Nichol, J.E.; Chan, P.W. Historical GIS Data and Changes in Urban Morphological Parameters for the Analysis of Urban Heat Islands in Hong Kong. *Int. Arch. Photogramm. Remote Sens. Spat. Inf. Sci.* **2016**, *XLI-B2*, 55–62. [[CrossRef](#)]
33. Shi, Y.; Ren, C.; Wu, E. Analysis of Urban Design Strategies Based on the Outdoor Wind Environment and Thermal Comfort—A Case Study of Beijing Xidan Commercial District. *J. Urban Plan.* **2012**, *5*, 92–98. [[CrossRef](#)]
34. Chen, J. Research on the Urban Surface Thermal Environment by Considering 3D Spatial Information: A Case Study of Nanjing City, China. *Geogr. Geo-Inf. Sci.* **2019**, *35*, 126. [[CrossRef](#)]
35. Jia, Q. Research Process on Urban Three-Dimensional Space Shape and Thermal Environmental Effects. *Archit. Cult.* **2018**, *2*. [[CrossRef](#)]

36. Zhou, W.; Tian, Y. Effects of urban three-dimensional morphology on thermal environment: A review. *Acta Ecol. Sin.* **2020**, *40*, 416–427. [[CrossRef](#)]
37. Chen, Y.; Shan, B.; Yu, X. Study on the spatial heterogeneity of urban heat islands and influencing factors. *Build. Environ.* **2021**, *208*, 08604. [[CrossRef](#)]

Disclaimer/Publisher’s Note: The statements, opinions and data contained in all publications are solely those of the individual author(s) and contributor(s) and not of MDPI and/or the editor(s). MDPI and/or the editor(s) disclaim responsibility for any injury to people or property resulting from any ideas, methods, instructions or products referred to in the content.